Dielectric, ultraviolet/visible, and Raman spectroscopic investigations of the phase transition sequence in $0.71Pb(Mg_{1/3}Nb_{2/3})O_3$-$0.29PbTiO_3$ crystals

H. Katzke,[1] M. Dietze,[1] A. Lahmar,[1] M. Es-Souni,[1,*] N. Neumann,[2] and S.-G. Lee[3]

[1]*Institute of Material and Surface Technology, University of Applied Science Kiel, Gernzstr. 3, DE-24149 Kiel, Germany*

[2]*InfraTec GmbH, Gostritzer Str. 61-63, DE-01217 Dresden, Germany*

[3]*IBULE Photonics, 7-39, Songdo dong, Yeonsu-gu, Incheon, 406-840, Republic of Korea*

(Received 25 October 2010; revised manuscript received 2 May 2011; published 31 May 2011)

The structural changes of $0.71Pb(Mg_{1/3}Nb_{2/3})O_3$-$0.29PbTiO_3$ (PMN-29PT) are studied by dielectric and optical absorption and hard-mode Raman spectroscopy as a function of temperature. In addition to the known phase transitions of this material at 100, 110 and 124 °C two new transitions at 42 and 60 °C are observed in unpoled [111]-oriented PMN-29PT single crystals. The phase transitions are associated with changes of the dielectric and optical properties arising from small changes of the inherent local symmetry. The experimental results are analyzed theoretically and a model for the temperature-dependent rotation of the spontaneous polarization is proposed. The formation of two new low-temperature phases, at least on a local scale, reflect an underlying polarization rotation path being much more complex than currently believed.

DOI: 10.1103/PhysRevB.83.174115 PACS number(s): 77.84.Ek

I. INTRODUCTION

In the last decade single crystals of (1-x)$Pb(Mg_{1/3}Nb_{2/3})O_3$-x$PbTiO_3$ (PMN-PT) have emerged as highly promising multifunctional materials with excellent electromechanical and electrooptical properties, particularly for compositions close to the morphotropic phase boundary (MPB).[1–4] The applications range from wave guides to ultrasonic transducers for high-performance ultrasonic imaging in diagnostics.[4–6] In the [111] orientation PMN-PT single crystals possess excellent pyroelectric properties making them interesting candidates for pyroelectric detectors with sensitivities that could match those of deuterated tryglicine sulphate single crystals (DTGS), which are the materials with the best known sensitivity yet combining high robustness and chemical stability.[7] These excellent properties probably originate from structural features inherent to the MPB first discovered in the $PbZrO_3$-$PbTiO_3$ (PZT) system.[8–10] In particular, the discovery of two intermediate monoclinic ferroelectric phases being thought to mediate the structural transition from rhombohedral to tetragonal has offered a suitable framework for correlating crystal chemistry and physical properties observed in the MPB region.[11–16] Vanderbilt and Cohen have shown in their pioneering theoretical work[17] that three types of monoclinic structures, namely M_A ($P_x = P_y \neq P_z$, $P_z > P_x$) and M_B ($P_x = P_y \neq P_z$, $P_z < P_x$) with Cm symmetry and M_C with Pm symmetry, are stable in the MPB composition range, stimulating extensive experimental work to prove their existence using different techniques.[11–15] Ye *et al.* have investigated the effect of poling and report that the monoclinic M_A-type phase appears at room temperature in poled PMN-35PT crystals under an electric field of 43 kV/cm while in crystals poled under electric fields below 5 kV/cm the rhombohedral phase predominated.[18] Yang *et al.* reported an electric-field-induced $M_C \rightarrow M_A$ phase transition in a PMN-33PT single crystal investigated by polarized micro-Raman spectroscopy.[19] Temperature-dependent studies by Bao *et al.* claimed the coexistence of monoclinic M_A- and M_C-type phases in a PMN-32PT single crystal at room temperature. The transition sequence taking place during heating is reported to be $M_A \rightarrow M_C \rightarrow C$.[20]

In the present work we present a systematic study of the phase transitions in an [111]-oriented single crystal of $0.71Pb(Mg_{1/3}Nb_{2/3})O_3$-$0.29PbTiO_3$ using x-ray diffraction, temperature-dependent dielectric properties, and ultraviolet/visible (UV/VIS) and Raman spectroscopy. We show that two low-temperature phases are stabilized in unpoled [111]-oriented PMN-29PT. The phase transitions are analyzed theoretically in the framework of the Landau theory of phase transitions. This approach reveals unifying schemes for the transition mechanisms allowing us to propose a self-consistent model for the underlying polarization rotation path.

II. EXPERIMENTAL

$0.71Pb(Mg_{1/3}Nb_{2/3})O_3$-$0.29PbTiO_3$ (PMN-0.29PT) single crystals are grown from the melt by a modified Bridgman technique.[21] [111]-oriented crystals are cut into square pieces of $0.5 \times 0.5 \times 0.03$ cm^3 and polished using a diamond suspension. The electrical poling is performed at 80 °C under an electric field of 10 kV/cm for 30 min followed by a slow cooling process to room temperature under an applied electric field. Depoling of the crystal is performed by heating it with 2K/min to 200 °C, holding it for 30 min at this temperature, following with a slow cooling process with less than 2K/min to ambient temperature. Dielectric measurements are performed at 1, 10, and 100 kHz with a computer-controlled Agilent 4192A impedance analyzer equipped with a hot stage ensuring a temperature control of ± 0.5 K. The ac-driving-signal amplitude was 100 mV.

X-ray diffraction studies are performed with a Bragg-Brentano diffractometer (by PanAnalytical X'Pert PRO MPD, Netherlands) operating in the Θ/2Θ mode using monochromatic Cu K_α radiation ($\lambda = 1.5406$ Å). Optical properties are measured at different temperatures using a ultraviolet/visible/near infrared (UV/VIS/NIR) spectrophotometer (by Lambda35, Perkin Elmer) equipped with a homemade heating

stage ensuring a temperature control of ± 0.5 K. Temperature-dependent Raman spectra are recorded with a SENTERRA Raman microscope spectrometer (by Bruker, Germany) at 536 nm excitation wavelength and a laser power of 20 mW. The temperature is controlled to ±0.5 K and the instrumental resolution is around 3 cm^{-1}. Raman band positions and intensities are evaluated by fitting the spectra using the software package OPUS 6.5 (by Bruker, Germany).

III. RESULTS

A. Dielectric properties

Figure 1 represents the dielectric constant and the dielectric loss of a PMN-29PT single crystal at 1, 10, and 100 kHz as a function of temperature. The poled crystal [see Fig. 1(a)] shows two sharp phase transitions at 100 and 110 °C, followed by a broad $\epsilon(T)$ peak centered at 124 °C with a maximum dielectric constant of 40 000. Such diffuse ferroelectric-paraelectric phase transition is typical for relaxor ferroelectrics and can be attributed to atomic disorder and compositional fluctuations in the crystal.[22] The unpoled crystal [see Fig. 1(b)] exhibits

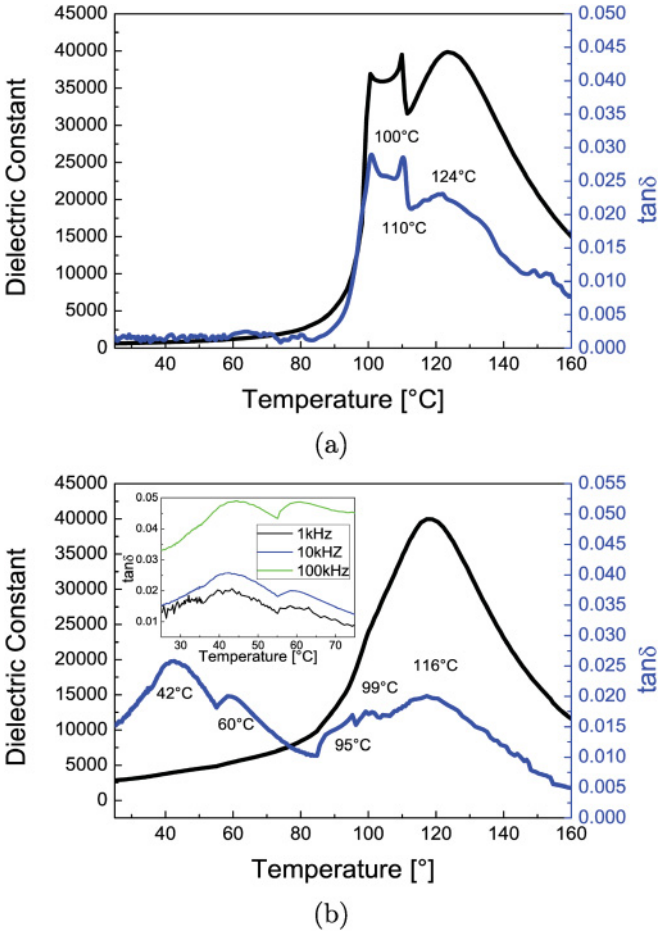

FIG. 1. (Color online) Temperature dependence of the dielectric constant ϵ and the dielectric loss tan δ for a PMN-29PT single crystal measured at 10 kHz for (a) poled crystal and (b) unpoled crystal. The inset in panel (b) shows the dielectric loss in the low-temperature range for different frequencies: 1 (black), 10 (blue), and 100 kHz (green).

five dielectric anomalies, at 42, 60, 95, 99, and 116 °C in the dielectric loss, whereas the dielectric-constant measurement shows only one broad peak centered at 116 °C with a maximum of 40 000. It is well known that the dielectric behavior of a crystal is very sensitive to structural changes, therefore, the dielectric-loss peaks can be assigned to phase transitions in the material occurring as a function of temperature. The two sharp anomalies at 100 and 110 °C for the poled crystal and 95 and 99 °C for the unpoled crystal are assigned to the monoclinic → monoclinic and monoclinic → tetragonal phase transitions whereas the broad anomalies at 124 °C and 116 °C are related to the ferroelectric → paraelectric phase transition in PMN-PT, respectively. For the unpoled sample two further low-temperature anomalies are observed at 42 and 60 °C. To our knowledge it is the first time that low-temperature anomalies are reported to occur in permittivity measurements of unpoled PMN-PT compounds. Frequency-dependent measurements show no shift in the peak temperatures for these anomalies, revealing that relaxation processes can be discarded as a possible explanation for their occurrence.

B. X-ray diffraction studies

The x-ray diffraction patterns of the poled and unpoled PMN-29PT single crystal are shown in Fig. 2(a). Due to the fact that the single crystal is oriented along the pseudocubic [111] direction, the information content of the powder x-ray diffraction studies is limited to the pseudocubic *hhh* reflections. Figure 2(a) shows the splitting of the pseudocubic 111 reflection and a significant intensity change after poling, indicating a field-induced structural phase transition. Figure 2(b) shows the calculated intensities for the rhombohedral $R3m$ phase, the monoclinic M_A and M_B phases with Cm symmetry, the monoclinic M_C phase with Pm symmetry, and the cubic $Pm\bar{3}m$ phase, assuming a single-crystal preferred orientation along the pseudocubic [111] direction for all phases. The experimental intensities for the poled crystal are in accordance with the calculated intensities for the monoclinic Cm phases, whereas a rhombohedral structure is found for the unpoled crystal in accordance with previous studies.[23]

C. UV/VIS spectroscopy

The optical transmittance spectra of a poled [111]-oriented PMN-29PT single crystal in the visible and near UV regions are shown in Fig. 3 at different temperatures. The crystal is all transparent in the visible region and rolls off near 450 nm, and it becomes completely absorbing around 390 nm, indicating an optical absorption edge in near UV. With increasing temperature the maximum transmittance increases from 64.5% at 25 °C to 66.9% at 125 °C and the short-wavelength cutoff becomes sharper. The transmittance at 800 nm is shown as a function of temperature in Fig. 4(a). The transmittance is more or less constant with a slight increase from 61.0% at 25 °C to 62.6% at 125 °C. When the sample is cooled down to room temperature, the transmittance follows the heating curve down to 90–100 °C; below 90 °C the transmittance decreases significantly from 61.8% to 54.2% at 30 °C, indicating that the phase behaviors are different for heating and cooling conditions. The following reasons can

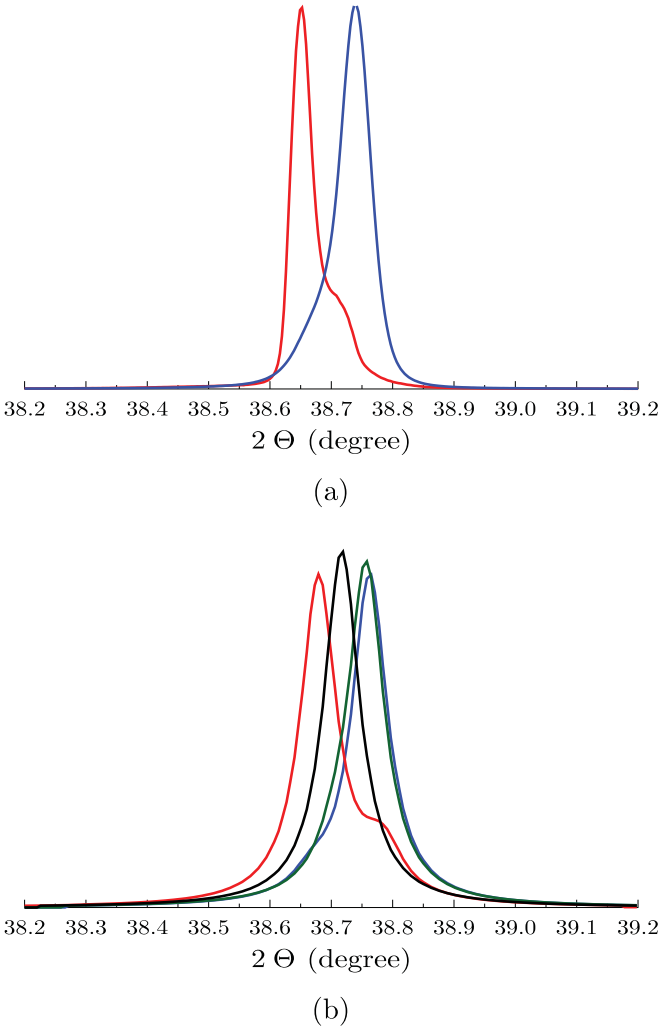

FIG. 2. (Color online) (a) X-ray diffraction patterns for a PMN-29PT single crystal before (blue curve) and after poling (red curve) at 10 kV/cm, showing the splitting of the pseudocubic 111 diffraction peak. (b) Calculated intensities for the cubic $Pm\bar{3}m$ phase (black curve), the rhombohedral $R3m$ phase (blue curve), the monoclinic M_A and M_B phases with Cm symmetry (red curve), and the monoclinic M_C phase with Pm symmetry (green curve), assuming a single-crystal preferred orientation along the pseudocubic [111] direction for all phases. The preferred orientation is modelled by applying a Rietveld-Toraya plate model with plane indices $(111)_C$, $(021)_R$, $(\bar{2}01)_{M_A,M_B}$, and $(111)_{M_c}$ and using the program POWDERCELL.[24] The peak profile is modelled with a Lorentzian-peak shape function.

be assigned for such a behavior: (1) the phase paths which are followed during heating and cooling can be different, not all of the phase transitions are reversible. (2) The domain structure of the poled crystal with well-aligned stripe-like microdomains is quite different from that of the unpoled crystal, which after heating shows randomly oriented nanodomains. The change of the domain structure is irreversible, the smaller size of the domains and the higher amount of domain walls influence the optical properties negatively and reduce the overall transmittance in the UV/VIS/NIR spectral range. The optical absorbance, defined as $A = -\log_{10} T = \epsilon_\lambda cd$, with c being the concentration of the absorbing species

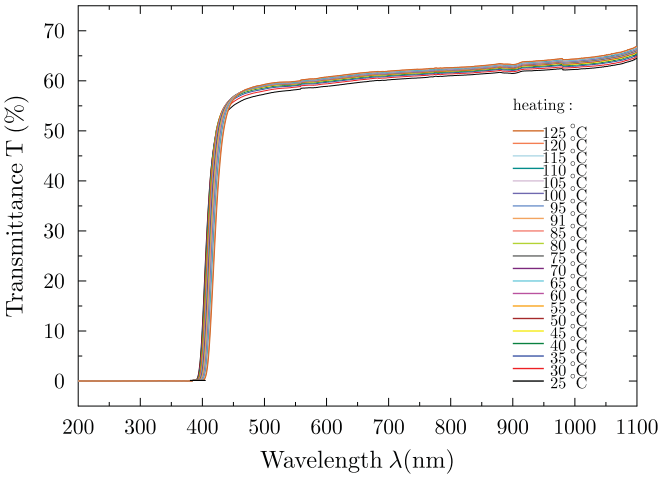

FIG. 3. (Color online) Optical transmittance spectra of a [111]-oriented poled PMN-29PT single crystal measured at different temperatures.

and d being the crystal thickness, is shown in Fig. 4(b). Variables c and d are constant as a function of temperature. Assuming a linear temperature dependence of the extinction coefficient, ϵ_λ, as validated for various types of materials in a large temperature range,[25–27] deviations from a linear fit indicate structural changes in the material as, for example,

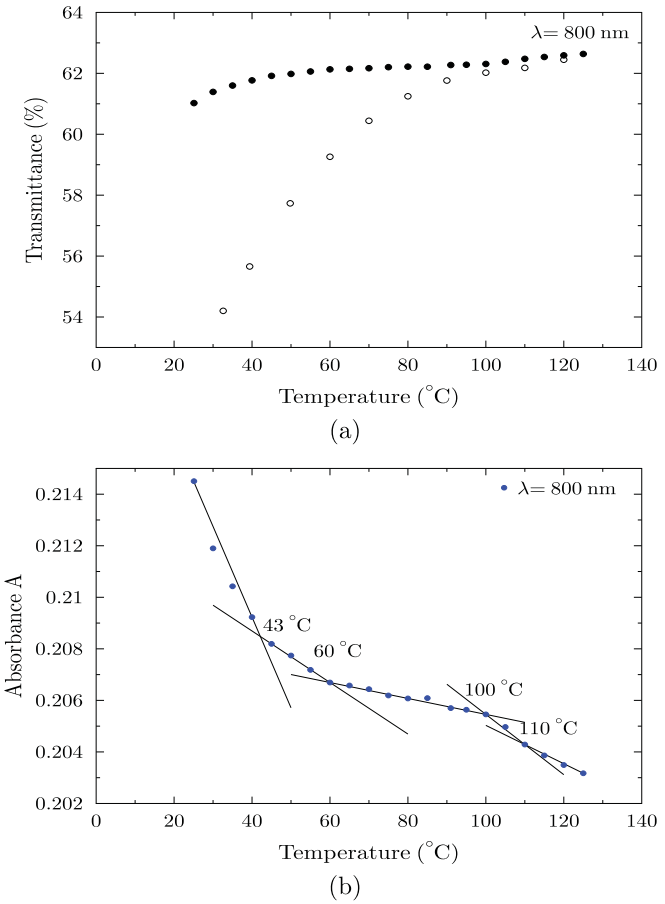

FIG. 4. (Color online) Transmittance (a) and absorbance (b) of a [111]-oriented poled PMN-29PT single crystal at 800 nm.

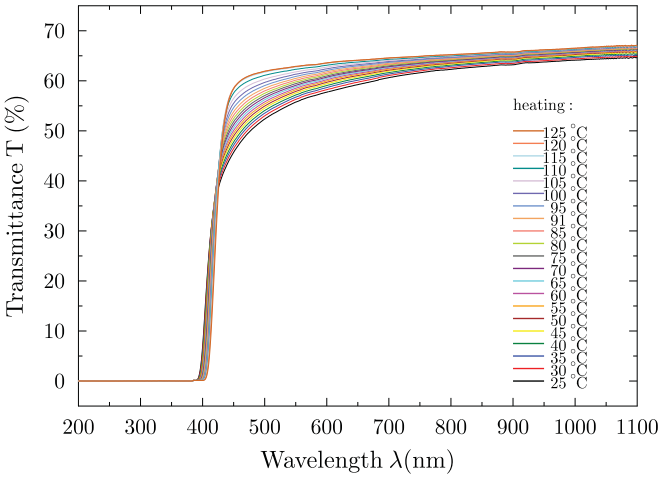

FIG. 5. (Color online) Optical transmittance spectra of a [111]-oriented unpoled PMN-29PT single crystal measured at different temperatures.

found for the ferroelectric → paraelectric phase transition in lead-germanium-telluride thin films.[28] Four deviations from linearity at 43, 60, 100, and 110 °C are found at 800 nm. These breaks in slope indicate small changes of the optical properties and thus point to structural changes. The transition temperatures at 100 and 110 °C are in accordance with the peaks in the dielectric measurement shown in Fig. 1(a). The low-temperature anomalies at 43 and 60 °C might be suggested but are not clearly resolved by dielectric measurements.

The optical transmittance spectra of the unpoled state are shown in Fig. 5 at different temperatures. Again, the crystal is all transparent in the visible region and it rolls off near 450 nm before becoming completely absorbing around 390 nm. With increasing temperature the maximum transmittance increases from 64.7% at 25 °C to 67.1% at 125 °C and the short-wavelength cutoff becomes significantly sharper. The transmittance at 800 nm is shown as a function of temperature in Fig. 6(a). The change of the optical properties as a function of temperature is less pronounced for the unpoled crystal, showing similar curves for the heating and cooling run. At 800 nm the transmittance of the unpoled crystal is by 1.3% higher than that of the poled crystal, and it increases by 3% from 62.3% at 25 °C to 65.2% at 125 °C. The optical absorbance at 800 nm is shown in Fig. 6(b). Four deviations from a linear dependence are found at 43, 62, 95, and 115 °C. The transition temperatures are in accordance with the peaks of the dielectric measurement shown in Fig. 1(b).

D. Raman scattering

Figure 7 represents the Raman spectra of the poled and unpoled PMN-29PT single crystal at room temperature. Broad peaks around 101, 120, 220, 272, 430, 511, 570, 753, and 802 cm^{-1} are observed for both unpoled and poled crystals. The single bands at 101 and 120 cm^{-1} are assigned to Pb-O and B-O motions while the broad 272 cm^{-1} band is assigned to the bending mode of O-B-O bonds. The weak peak near 430 cm^{-1} is attributed to Mg-O-Mg vibrations. The doublets observed in the high-frequency regions around 540 and 780 cm^{-1} are characteristic of perovskites with different B

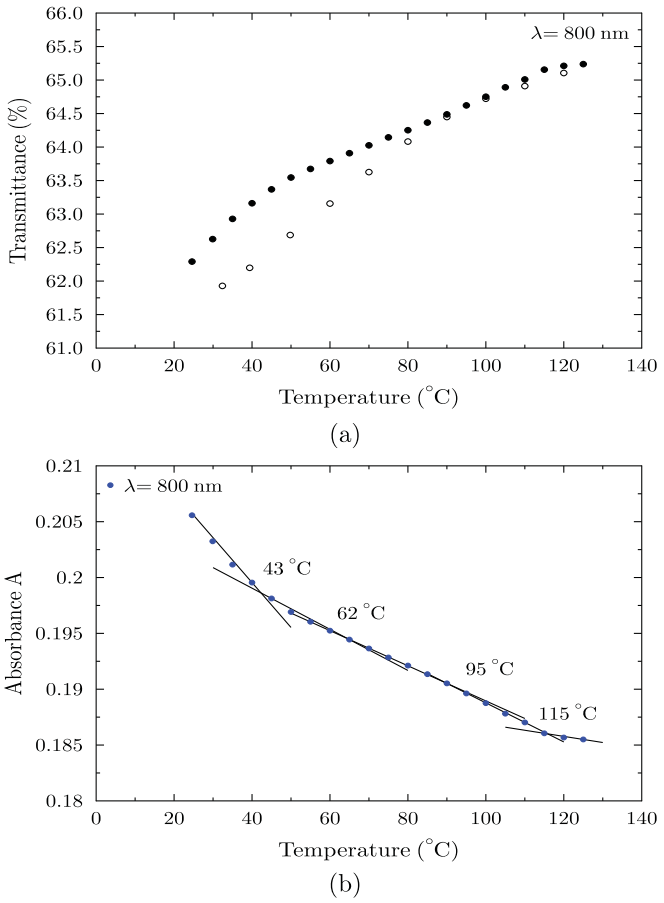

FIG. 6. (Color online) Transmittance for heating and cooling (a) and absorbance with increasing temperature (b) of a [111]-oriented unpoled PMN-29PT single crystal at 800 nm.

cations and are related to the B′-O-B″ bending and stretching modes, respectively. By considering the mass effect, the higher and lower frequencies are related to the Ti-O and Mg/Nb-O bonds, respectively.[29–31] After poling, the intensities of the shoulder peak at 511 cm^{-1} and the doublet peak at 780 cm^{-1} significantly increase, which was reported by Yang et al. to be a signature of the existence of the M_A-type monoclinic structure.[19]

Figure 8 shows Raman spectra of a poled [111]-oriented PMN-29PT single crystal as a function of temperature. Despite the fact that the paraelastic phase above the ferroelectric-paraelectric phase transition is assumed to adopt a centrosymmetric structure with $Pm\bar{3}m$ symmetry, a Raman spectrum exists at all temperatures far above the Curie temperature indicating that the local translational and (or) rotational symmetry is broken at all temperatures. Since the Raman spectra do not show drastic spectral changes, the evolution of the frequency and intensity for these Raman bands is analyzed as a function of temperature. According to the concept of hard-mode Raman spectroscopy,[32–35] these bands should be sensitive to structural changes. The 400 to 700 cm^{-1} region is composed of three bands, two dominating splitted bands and one underlying single band. The frequency shifts and the intensities of the Raman bands around 430 and 753 cm^{-1} are shown in Figs. 9(a)– 9(d). Hard-mode features are slightly

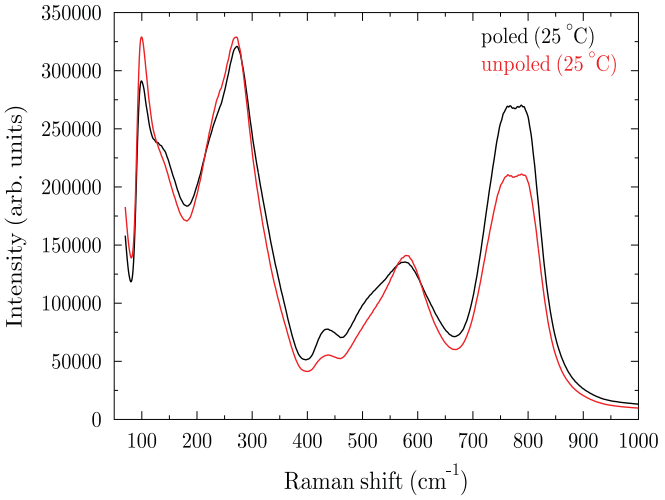

FIG. 7. (Color online) Raman spectra of a poled and unpoled PMN-29PT single crystal at room temperature.

seen and, generally, more or less pronounced depending on the particular phonon. The latter point can be easily verified in Fig. 9 showing that spectral changes are clearly visible for some plots while they are less pronounced in others. The Raman band at around 430 cm^{-1} is showing a clear low-frequency shift in the temperature range 25 °C $\leqslant$ T $\leqslant$ 97 °C. Between 97 and 105 °C the frequency is constant, before the mode hardens up to 130 °C. For temperatures above 130 °C the frequency remains constant. The change in the frequency shift is accompanied by a change in intensity, shown in Fig. 9(b). Three deviations from a linear decrease are observed at 97, 105, and 130 °C corresponding well with the changes in slope of the frequency shift shown in Fig. 9(a). The frequency shift of the Raman band at around 753 cm^{-1} shows three less pronounced discontinuities at 97, 105, and 125 °C corresponding to intensity changes at 97, 110, and 120 °C.

The Raman spectra of the unpoled [111]-oriented PMN-29PT single crystal are shown at different temperatures in Fig. 10 and the frequency shifts and intensities of the Raman

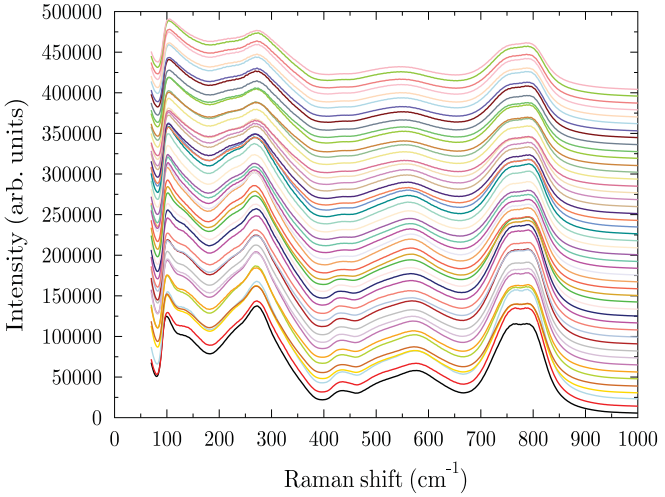

FIG. 8. (Color online) Hard-mode Raman spectra of a poled PMN-29PT single crystal measured at different temperatures from 25 to 260 °C in steps of 5 °C.

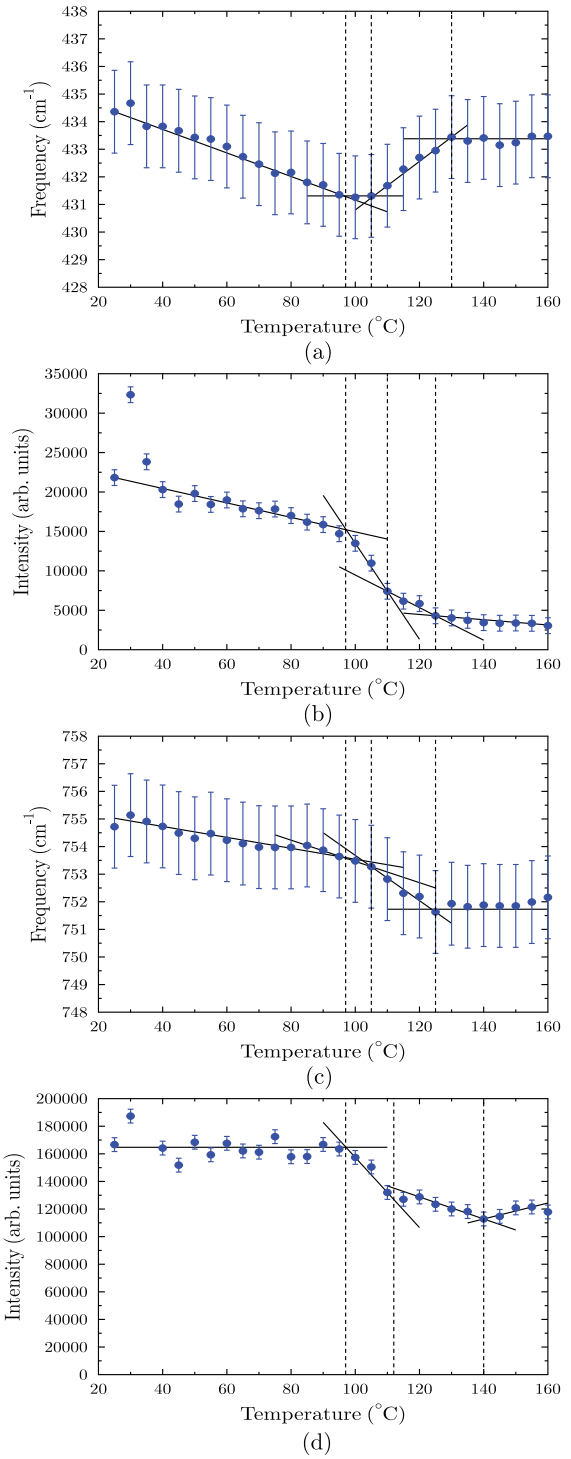

FIG. 9. (Color online) (a)–(d) Frequency shift and integrated intensities vs temperature of the modes near 430 and 753 cm^{-1} for a poled PMN-29PT single crystal.

bands at 430 and 753 cm^{-1} are shown in Figs. 11(a)–11(d). Pronounced spectral changes become only visible in the intensities of the Raman modes at 430 and 753 cm^{-1}, whereas the frequency shift is constant within the instrumental resolution of 3 cm^{-1}. The temperature dependence of the intensities shows changes in the slope at 58–60, 85–87, 97–99, and 110–115 °C.

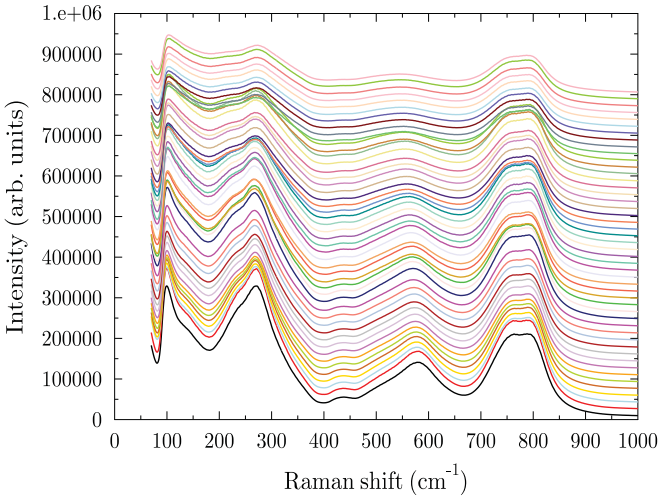

FIG. 10. (Color online) Hard-mode Raman spectra of an unpoled PMN-29PT single crystal measured at different temperatures from 25 to 260 °C in steps of 5 °C.

Figure 12 compares the Raman spectra of the poled and unpoled crystal at 50, 70, 90, and 110 °C. While the Raman spectra are essentially different for temperatures below 110 °C, they are identical for all temperatures above 110 °C, indicating a similar structure above the ferroelectric-paraelectric phase transition temperature for the poled and unpoled crystal.

Raman scattering is a well-suited technique for the investigation of local lattice distortions on an atomic scale. Polyhedron distortions in oxides are known to result in a high-frequency shift.[36–39] The slightly higher frequencies of the modes (by 1–2 cm^{-1}) around 430 and 753 cm^{-1} of the poled crystal indicate a higher degree of polyhedral distortion in the structure of the poled sample. All bands show a low-frequency shift with increasing temperature. The only exception is the band at 430 cm^{-1}, which hardens between 105 and 130 °C. The softening of the modes with increasing temperature is in accordance with the assumption that the paraelectric high-temperature phase is of higher symmetry and less distorted, whereas the hardening of the 430 cm^{-1} mode indicates the formation of an intermediate phase with a higher degree of polyhedral distortion.

IV. DISCUSSION

A. Phase transition sequence in PMN-29PT

Dielectric, optical UV/VIS, and Raman spectroscopic investigations suggest a complex phase-transition sequence in poled and unpoled PMN-29PT as a function of temperature with the formation of several intermediate phases before reaching the paraelectric cubic phase. Figure 13 shows the proposed phase-transition sequence for poled and unpoled PMN-29PT as a function of temperature. At ambient temperature poled PMN-29PT possesses a monoclinic M_A-type structure that transforms at 100 °C into a monoclinic M_C-type structure. The phase transition at 110 °C is assigned to the transformation of the monoclinic M_C phase into the tetragonal phase, which finally transforms at 124 °C into the cubic phase having an average macroscopic symmetry of $Pm\bar{3}m$.

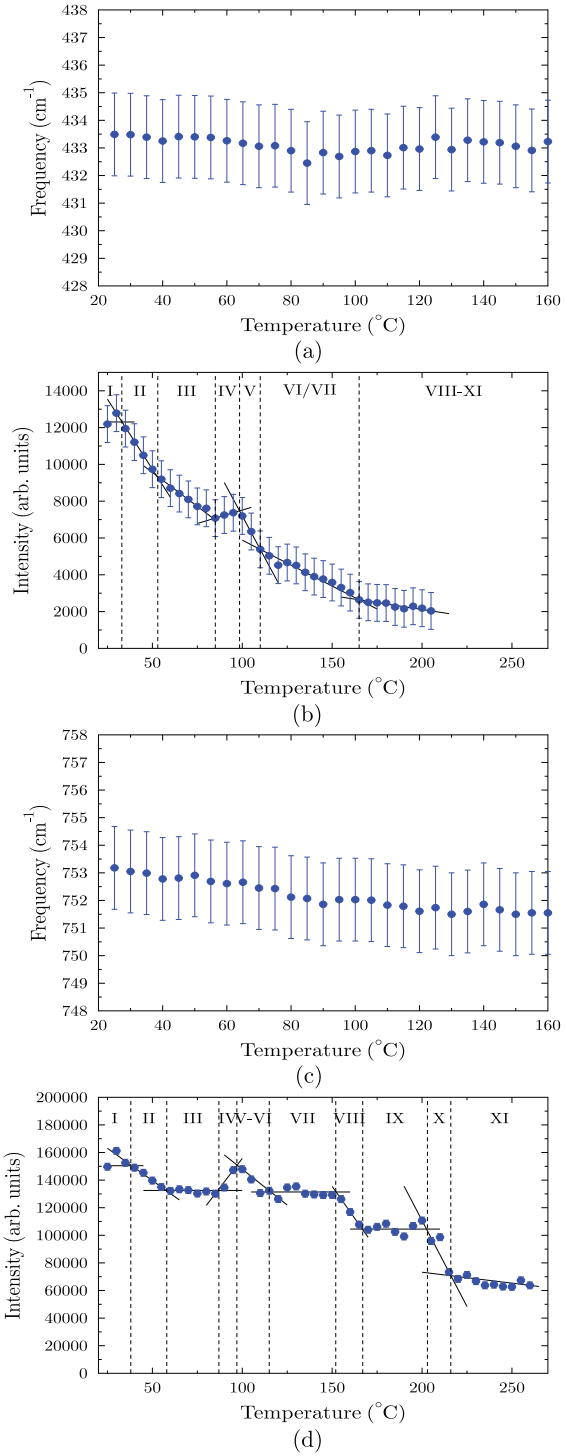

FIG. 11. (Color online) (a)–(d) Frequency shift and integrated intensities vs temperature of the modes near 430 and 753 cm^{-1} for an unpoled PMN-29PT single crystal.

The unpoled crystal exhibits a rhombohedral structure at room temperature. Two low-temperature phase transitions at 42 and 60 °C are observed in unpoled PMN-29PT. These phase transitions are assigned to the rhombohedral R → M_B and M_B → O transitions. The orthorhombic O phase transforms at 95 °C into the monoclinic M_C phase that transforms at 99 °C into the tetragonal T and at 116 °C into the cubic C phase.

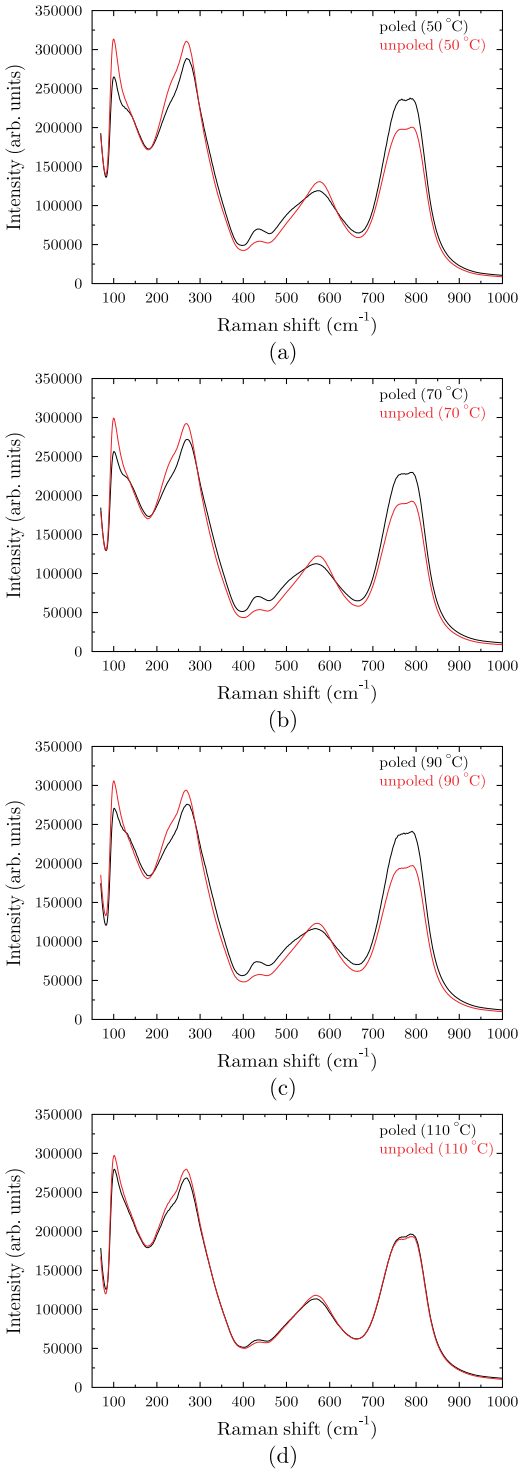

FIG. 12. (Color online) Raman spectra of a poled and unpoled PMN-29PT single crystal at (a) 50, (b) 70, (c) 90, and (d) 110 °C.

B. Group-theoretical analysis

A group-theoretical analysis is now performed in order to rationalize the experimental observations ensuing the phase transformations depicted above. The ideal structure of perovskite-type ABO_3 oxides is essentially simple possessing corner-linked BO_6 octahedra with the B cations at the center of the octahedra and the A cations in cuboctahedral voids between the octahedra. In PMN-PT the B site is occupied

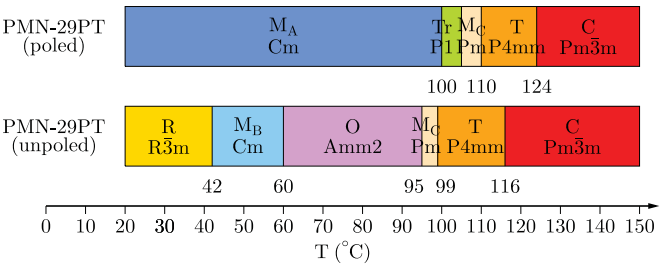

FIG. 13. (Color online) Proposed phase-transition sequence in poled and unpoled PMN-29PT as a function of temperature.

by either magnesium, niobium, or titanium. Fully disordered PMN-PT possesses cubic $Pm\bar{3}m$ symmetry. According to the selection rules of $Pm\bar{3}m$ symmetry no mode should be Raman active (see Table I). Ordering is known to be favored in the octahedral B site because there is a substantial charge difference between the three cation species Mg^{2+}, Nb^{5+}, and Ti^{4+}. Different ordering schemes are discussed in order to explain the appearance of the intense Raman spectrum in the paraelectric $Pm\bar{3}m$ cubic phase. Husson *et al.*,[41] Bismayer *et al.*,[42] and Kania *et al.*[43] explained the origin of the Raman spectrum of the cubic phase of complex perovskites by the existence of ordered $Fm\bar{3}m$ clusters with 1:1 order of Mg and Nb in the B sublattice. Svitelskiy *et al.*[44] suggest that the PMN-PT Raman spectrum can originate both from the $Fm\bar{3}m$ clusters and microscopic polar $R3m$ nanoregions, which are rich in Mg, Nb, or Ti, thermodynamically in nonequilibrium, thus breaking the translational symmetry. To the best of our knowledge, there has been so far no convincing experimental evidence for a long-range ordered phase, therefore for the group-theoretical analysis the average symmetry of the paraelectric phase is assumed to be $Pm\bar{3}m$, and the observed Raman activity is attributed to the existence of polar nanoregions.

The five atoms in both the rhombohedral $R3m$ and tetragonal $P4mm$ unit cells of the ferroelectric PMN-PT phases below the Curie temperature give rise to nine ($\Gamma_{\text{Raman}} = 4A_1 + 5E$) and ten ($\Gamma_{\text{Raman}} = 4A_1 + 1B_1 + 5E$) Raman-active phonon modes, respectively. For the low-symmetry orthorhombic, monoclinic, and triclinic structures with $Amm2$, Cm, Pm, and $P1$ symmetries, 15 Raman-active phonon modes are symmetry allowed. A detailed overview of the symmetry and activity

TABLE I. Group-theoretical analysis of the phonon modes in space group $Pm\bar{3}m$ (221). The symmetry-adapted modes for the Γ point were calculated using the Bilbao crystallographic server.[40]

Atom	Wyckoff position	Site symmetry	$m\bar{3}m$ factor group representation	
			T_{2u}	T_{1u}
Pb	1a	$m\bar{3}m$		1
Ti/Nb/Mg	1b	$m\bar{3}m$		1
O	3c	$4/mm.m$	1	2
		Γ_{total}	1	4
		Γ_{IR}		4
		Γ_{Raman}		

TABLE II. Group-theoretical analysis of the phonon modes in space group $R3m$ (160). The symmetry-adapted modes for the Γ point were calculated using the Bilbao crystallographic server.[40]

Atom	Wyckoff position	Site symmetry	$3m$ factor group representation		
			A_1	A_2	E
Pb	1a	$3m$	1		1
Ti/Nb/Mg	1a	$3m$	1		1
O	3b	$.m$	2	1	3
		Γ_{total}	4	1	5
		Γ_{IR}	4		5
		Γ_{Raman}	4		5

of the different modes in these structures are summarized in Tables II– VII.

Figure 14 gives the correlation between the phonon modes of the symmetry groups involved in the proposed transformation process. The number of Raman-active phonon modes is identical for the orthorhombic, monoclinic, and triclinic structures and reduces theoretically from 15 to 9, and 10, respectively, with increase of the symmetry to $R3m$ or $P4mm$ symmetries. The invariant number of Raman-active phonon modes for the low-symmetry structures is the reason why only small changes of the Raman spectra are observed as a function of temperature.

The thermodynamic paths relating the different structures, depicted in Fig. 13, are shown in Fig. 15. The simple cubic $Pm\bar{3}m$ phase can be taken as the parent structure from which all other structures can be deduced by critical instabilities. During the $Pm\bar{3}m \rightarrow R3m$ transformation the unit cell remains unchanged in size and hence the critical point of the Brillouin zone of the paraphase is the Γ point. According to Stokes and Hatch,[45] the active representation that accounts for the symmetry lowering $Pm\bar{3}m \rightarrow R3m$ is Γ_4^-. The spontaneous physical quantities transforming according to this irreducible representation are the elastic deformation with the proper components $e_{yz} = e_{zx} = e_{xy}$ and the spontaneous polarization parallel to z below T_c. In the same way, symmetry reductions to tetragonal $P4mm$, orthorhombic $Amm2$, monoclinic Cm, monoclinic Pm, and triclinic $P1$ symmetries can theoretically be constructed using the same active representation that transforms as Γ_4^-.[45]

TABLE III. Group-theoretical analysis of the phonon modes in space group $P4mm$ (99). The symmetry-adapted modes for the Γ point were calculated using the Bilbao crystallographic server.[40]

Atom	Wyckoff position	Site symmetry	$4mm$ factor group representation				
			A_1	A_2	B_1	B_2	E
Pb	1a	$4mm$	1				1
Ti/Nb/Mg	1b	$4mm$	1				1
O1	1b	$4mm$	1				1
O2	2c	$2mm.$	1		1		2
		Γ_{total}	4		1		5
		Γ_{IR}	4				5
		Γ_{Raman}	4		1		5

TABLE IV. Group-theoretical analysis of the phonon modes in space group $Amm2$ (38). The symmetry-adapted modes for the Γ point were calculated using the Bilbao crystallographic server.[40]

Atom	Wyckoff position	Site symmetry	$mm2$ factor group representation			
			A_1	A_2	B_1	B_2
Pb	2a	$mm2$	1		1	1
Ti/Nb/Mg	2b	$mm2$	1		1	1
O1	2a	$mm2$	1		1	1
O2	4e	$m..$	2	1	1	2
		Γ_{total}	5	1	4	5
		Γ_{IR}	5		4	5
		Γ_{Raman}	5	1	4	5

The trigonal $R3m$ and tetragonal $P4mm$ phases are not group-subgroup related, however, they are connected with each other via their common subgroup Cm identified as the symmetry of the monoclinic M_A and M_B phase. The active representations accounting for the symmetry lowering $R3m \rightarrow Cm$ and $P4mm \rightarrow Cm$ transform as Γ_3 and Γ_5, respectively. The $M_A \rightarrow M_C$ phase transition is reconstructive and the Cm and Pm space groups are not group-subgroup related. The transformation can proceed either via an orthorhombic O phase with $Amm2$ symmetry or via a triclinic phase with P1 symmetry. In the same way, a transformation from the orthorhombic O phase into the tetragonal T phase requires an intermediate phase with monoclinic symmetry being either of the M_A/M_B or M_C type.

C. Polarization rotation path

Figure 16 depicts the possible directions of the polarization vector and the corresponding symmetries of PMN-PT phases. The components of the spontaneous polarization are related for all phases to a pseudocubic unit cell. In the ferroelectric rhombohedral R phase the components of the spontaneous polarization are $P_x = P_y = P_z \neq 0$ corresponding to a polarization vector that is aligned along one of the cubic body diagonals (yellow line in Fig. 16). For $P_x = P_y \neq P_z \neq 0$ a monoclinic structure with Cm symmetry is formed, which is of the M_A type for $P_z > P_x$ and of the M_B type for $P_z < P_x$. The polarization vector lies in the plane that is indicated in blue

TABLE V. Group-theoretical analysis of the phonon modes in space group Cm (8). The symmetry-adapted modes for the Γ point were calculated using the Bilbao crystallographic server.[40]

Atom	Wyckoff position	Site symmetry	m factor group representation	
			A′	A″
Pb	2a	m	2	1
Ti/Nb/Mg	2a	m	2	1
O1	2a	m	2	1
O2	4b	1	3	3
		Γ_{total}	9	6
		Γ_{IR}	9	6
		Γ_{Raman}	9	6

TABLE VI. Group-theoretical analysis of the phonon modes in space group Pm (6). The symmetry-adapted modes for the Γ point were calculated using the Bilbao crystallographic server.[40]

Atom	Wyckoff position	Site symmetry	m factor group representation A′	A″
Pb	1a	m	2	1
Ti/Nb/Mg	1b	m	2	1
O1	1a	m	2	1
O2	1b	m	2	1
O3	1b	m	2	1
		Γ_{total}	10	5
		Γ_{IR}	10	5
		Γ_{Raman}	10	5

in Fig. 16. For $P_x = P_y \neq 0$, $P_z = 0$ an orthorhombic structure with $Amm2$ symmetry is formed. $Amm2$ structures are also obtained for $P_x = P_z \neq 0$, $P_y = 0$ and $P_x = 0$, $P_y = P_z \neq 0$. The three possible directions of the polarization vector are indicated by violet lines in Fig. 16. The symmetry is lowered to monoclinic Pm when one of the polarization components is zero, but the other two being different, i.e., $P_x \neq P_y \neq 0$, $P_z = 0$, $P_x = 0$, $P_y \neq P_z \neq 0$, and $P_x \neq P_z \neq 0$, $P_y = 0$. The polarization vector lies then in the a/b-, b/c-, or a/c-planes (beige planes in Fig. 16). If the polarization vector has only one nonvanishing component, a tetragonal structure with $P4mm$ symmetry is formed. The polarization vector points then along one of the three symmetry-equivalent axis of the pseudocubic unit cell (orange lines in Fig. 16). For general polarization components $P_x \neq P_y \neq P_z \neq 0$ the spontaneous polarization is unconstrained by symmetry, the resulting phase has triclinic $P1$ symmetry (all points inside the pseudocubic unit cell).

For unpoled [111]-oriented PMN-29PT the following polarization rotation path is proposed : R ($P_x = P_y = P_z \neq 0$) → M_B ($P_x = P_y \neq P_z \neq 0, P_z < P_x$) → O ($P_x = P_y \neq 0, P_z = 0$) → M_C ($P_x \neq P_y \neq 0, P_z = 0, P_x > P_y$) → T ($P_x \neq 0, P_y = P_z = 0$) → C ($P_x = P_y = P_z = 0$).

The polarization path that is followed by poled PMN-29PT is different from that of unpoled PMN-29PT. The following path can be proposed : M_A ($P_x = P_y \neq P_z \neq 0, P_z > P_x$) → Tr ($P_x \neq P_y \neq P_z \neq 0$) → M_C ($P_x = 0, P_y \neq P_z \neq 0$ or $P_x \neq P_z \neq 0, P_y = 0$) → T ($P_x = P_y = 0, P_z \neq 0$) → C ($P_x = P_y = P_z = 0$). For symmetry reasons a monoclinic M_A → M_C phase transition is not allowed to occur in one step. An intermediate phase is mandatory, and it should have the triclinic $P1$ symmetry, which was found to be stable, after Vanderbilt and Cohen,[17] when extending the Devenshire theory to twelfth order in the ferroelectric order parameter. The idea of an intermediate triclinic structure is further supported by Raman spectroscopic results indicating the formation of an intermediate phase with a higher degree of polyhedral distortion resulting in the observed hardening of the 430 cm^{-1} mode.

TABLE VII. Group-theoretical analysis of the phonon modes in space group $P1$ (1). The symmetry-adapted modes for the Γ point were calculated using the Bilbao crystallographic server.[40]

Atom	Wyckoff position	Site symmetry	1 factor group representation A
Pb	1a	1	3
Ti/Nb/Mg	1a	1	3
O1	1a	1	3
O2	1a	1	3
O3	1a	1	3
		Γ_{total}	15
		Γ_{IR}	15
		Γ_{Raman}	15

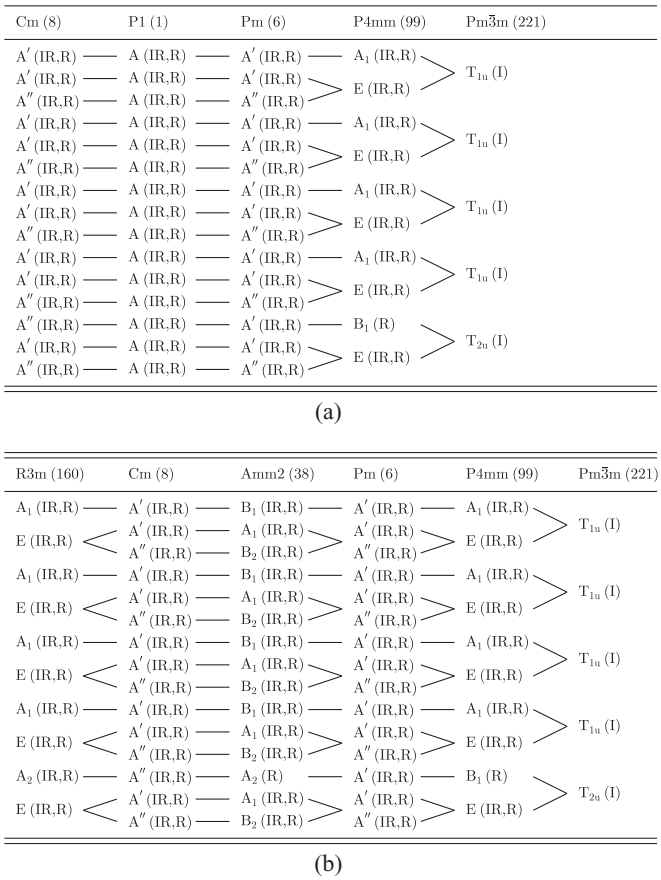

FIG. 14. Assignment of vibration modes in PMN-29PT structures. (a) Phase-transition sequence in unpoled PMN-29PT, (b) Phase-transition sequence in poled PMN-29PT.

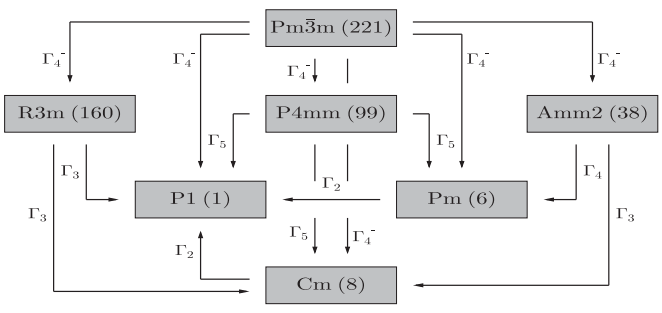

FIG. 15. Symmetry relationships between the structures observed in PMN-29PT as a function of temperature. The irreducible representations associated with the symmetry-breaking mechanisms are indicated. The notation of Stokes and Hatch is used.[45]

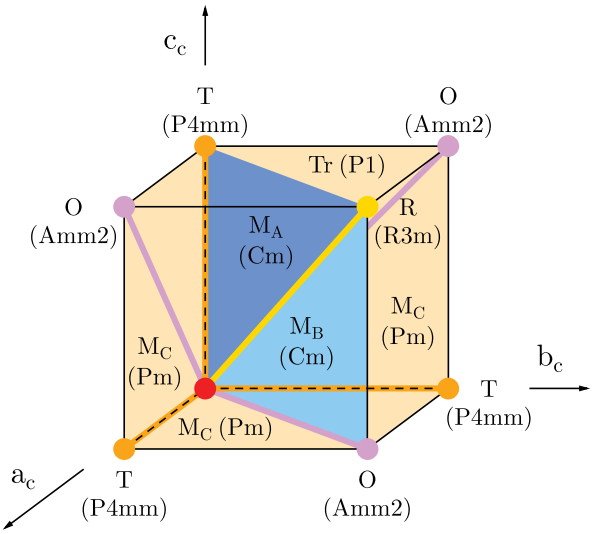

FIG. 16. (Color online) Illustration of the possible polarization rotation paths with the corresponding symmetries of the PMN-29PT phases.

Different polarization rotation paths are proposed in the literature depending on the direction of the electric field and the orientation of the crystal. An irreversible R → M_A → M_C → T phase sequence was observed for [001]-poled PMN-29.5PT by Guo *et al.*[46] An orthorombic O phase was observed in PMN-PT crystals poled along [110] and [111] directions but not along the [001] direction. Systemic studies of Li *et al.*[47] revealed a strong dependence of the phase path on the direction and strength of the electric field. For [110]-oriented single crystals a R → T → C sequence was observed under zero dc bias whereas for nonzero dc bias a phase sequence R → O → T → C was found. [001]- and [111]-oriented single crystals showed only the R → T and T → C transitions, whereas studies of Lin *et al.*[48] revealed a R → M_A → M_C → T → C phase sequence with increasing temperature in poled [001]-oriented PMN-30PT, whereas unpoled [001]-oriented PMN-30PT exhibits only one R → C phase transition. Poled [011]-oriented PMN-30PT crystals followed another phase path of R → M_B/O → T → C whereas unpoled [011]-oriented crystals showed only the direct transformation of the rhombohedral into the cubic phase.

Considering the illustration of the directions of the polarization vectors in the different phases it is obvious that poling the crystal along [111], [011], and [001] should have an influence on the path that is followed by the polarization rotation. The energy differences between the single phases are very small, this means that the appearance and stability of the intermediate phases as well as the phase transition paths that are followed strongly depend on external parameters such as the chemical composition, the domain structure, the mobility of domain walls, and, last but not least, on the applied electric field, which favors the stability of phases having a polarization vector close to the direction of the electric field.

V. SUMMARY AND CONCLUSIONS

In the present paper we have studied the structural phase transitions of PMN-29PT single crystals using x-ray diffraction, optical UV/VIS, and Raman spectroscopy. The phonon characteristics in PMN-29PT have been analysed by using the concept of hard-mode Raman spectroscopy, allowing the elucidation of spectral changes related to phase transitions of PMN-29PT. Any change in the crystal structure or the physical properties give rise to a variation in the phonon behavior, and the analysis of the frequency, intensity, and linewidth evolution of the whole spectra as a function of temperature gives insight into the change of phases. The phonon characteristics in PMN-29PT show pronounced changes between 25 and 160 °C. For the poled PMN-29PT single-crystal, transitions at 97–100, 105–112, and 125–140 °C are found, indicating a phase transition path of M_A → Tr → M_C → T → C. The transitions between 97 and 140 °C are clearly demonstrated by dielectric measurements and Raman spectroscopy. The stability range of the bridging triclinic phase is probably very small; it will be a challenging task to prove its existence by a temperature-dependent structural analysis. For the unpoled crystal, transitions at 42–43, 60–62, 85–95, 99, and 110–116 °C are detected, representing a transition path from the rhombohedral to the cubic phase via intermediate monoclinic and orthorhombic phases: R → M_B → O → M_C → T → C. All transitions are confirmed by at least two complementary methods.

The occurrence of additional low-temperature intermediate phases, as evidenced by dielectric, optical and Raman spectroscopy, is, in itself, not surprising. It has already been pointed out[49] that the structural changes from an *R*3*m* to a *P*4*mm* space group are very large (*R*3*m* and *P*4*mm* are not group-subgroup related) while an intermediate phase or phases could make such a change energetically more plausible. According to Bismayer,[42] the different symmetry-breaking steps in a sequence of phase transitions should be also considered. The formation of one or two intermediate phases, at least on a local scale, may reflect such a stepwise transition from a low-symmetry monoclinic to a high-symmetry cubic phase.

In summary, a structural phase transition is induced by applying an external electric field, as evidenced by x-ray diffraction, UV/VIS, and Raman spectroscopy. The poled crystal possesses probably a monoclinic structure with *Cm* symmetry, whereas the unpoled crystal exhibits a rhombohedral structure at ambient temperature. The complementary use of temperature-dependent dielectric measurements, optical UV/VIS, and Raman spectroscopy on PMN-29PT allows us to propose the existence of further low-temperature intermediate phases, which might be seen as bridge phases buffering the important rhombohedral-tetragonal symmetry change taking place as a function of temperature. Finally, we have conducted a rigorous group-theoretical analysis in order to corroborate the experimental observations. Nevertheless, further diffraction and spectroscopic work is necessary in order to determine the structures and/or local symmetries of the intermediate orthorhombic and triclinic phases.

ACKNOWLEDGMENTS

Financial support from the German Federal Ministry of Economics and Technology under contract No. KF2448901JT9 is gratefully acknowledged.

*mohammed.es-souni@fh-kiel.de

[1] S.-E. Park and T. R. Shrout, J. Appl. Phys. **82**, 1804 (1997).
[2] Y. Lu, D. Y. Jeong, Z. Y. Cheng, Q. M. Zhang, H. S. Luo, Z. W. Yin, and D. Viehland, Appl. Phys. Lett. **78**, 3109 (2001).
[3] J. Kuwata, K. Uchino, and S. Nomura, Jpn. J. Appl. Phys. **21**, 1298 (1982).
[4] L. E. Cross, Ferroelectrics **76**, 241 (1987).
[5] P. A. Whodkowski, K. Deng, and M. Kahn, Sensors and Actuators A **90**, 125 (2001).
[6] S. Kawamura, J. H. Kaneko, H. Fujimoto, Y. Otake, F. Fujita, A. Homma, T. Sawamura, P. Mikula, and M. Furusaka, Physics B: Condens. Matter **385-386**, 1277 (2006).
[7] R. B. Lal and A. K. Batra, Ferroelectrics **142**, 51 (1993).
[8] H. Fu and R. E. Cohen, Nature (London) **403**, 281 (2000).
[9] J. Kuwata, K. Uchino, and S. Nomura, Ferroelectrics **37**, 579 (1981).
[10] X.-H. Du, J. Zheng, U. Belegundu, and K. Uchino, Appl. Phys. Lett. **72**, 2421 (1998).
[11] B. Noheda, D. E. Cox, G. Shirane, S.-E. Park, L. E. Cross, and Z. Zhong, Phys. Rev. Lett. **86**, 3891 (2001).
[12] J.-M. Kiat, Y. Uesu, B. Dkhil, M. Matsuda, C. Malibert, and G. Calvarin, Phys. Rev. B **65**, 064106 (2002).
[13] B. Noheda, Curr. Opin. Solid State Mater. Sci. **6**, 27 (2002).
[14] B. Noheda, D. E. Cox, G. Shirane, J. Gao, and Z.-G. Ye, Phys. Rev. B **66**, 054104 (2002).
[15] A. A. Bokov and Z.-G. Ye, Phys. Rev. B **66**, 094112 (2002).
[16] A. K. Singh, D. Pandey, and O. Zaharko, Phys. Rev. B **68**, 172103 (2003).
[17] D. Vanderbilt and M. H. Cohen, Phys. Rev. B **63**, 094108 (2001).
[18] Z. G. Ye, B. Noheda, M. Dong, D. Cox, and G. Shirane, Phys. Rev. B **64**, 184114 (2001).
[19] Y. Yang, Y. L. Liu, S. Y. Ma, K. Zhu, L. Y. Zhang, J. Cheng, G. G. Siu, Z. K. Xu, and H. S. Luo, Appl. Phys. Lett. **95**, 051911 (2009).
[20] P. Bao, F. Yan, X. Lu, J. Zhu, H. Shen, Y. Wang, and H. Luo, Appl. Phys. Lett. **88**, 092905 (2006).
[21] H. Luo, G. Xu, H. Xu, P. Wang, and Z. Yin, J. Appl. Phys. **39**, 5581 (2000).
[22] M. E. Lines and A. M. Glass, *Principle and Applications of Ferroelectrics and Related Materials* (Claredon Press, Oxford, 1977).
[23] F. Bai, N. Wang, J. Li, D. Viehland, P. M. Gering, G. Xu, and G. Shirane, J. Appl. Phys. **96**, 1620 (2004).
[24] W. Kraus and G. Nolze, POWDERCELL, Version 2.4 (2000).
[25] B. M. Abraham and A. Jeannotte, Inorg. Chem. **16**, 2270 (1977).
[26] O. Yavas, N. Do, A. C. Tam, P. T. Leung, W. P. Leung, H. K. Park, C. P. Grigoropoulos, J. Boneberg, and P. Leiderer, Opt. Lett. **18**, 540 (1993).
[27] C. Marin, A. G. Ostrogorsky, G. Foulon, D. Jundt, and S. Motakef, Appl. Phys. Lett. **78**, 1379 (2001).
[28] B. Li, J. Jiang, S. Zhang, and F. Zhang, J. Appl. Phys. **91**, 3556 (2002).
[29] E. C. Prado, R. W. Tao, A. R. Guo, R. S. Katiyar, and A. S. Bhalla, Ferroelectrics Lett. **21**, 17 (1996).
[30] E. B. Ara'ujo, R. N. Reis, C. A. Guarany, C. T. Meneses, J. M. Sasaki, A. G. S. Filho, and J. M. Filho, Mater. Chem. Phys. **104**, 40 (2007).
[31] J. A. Lima, W. Paraguassu, P. T. C. Freire, A. G. Souza Filho, C. W. A. Paschoal, J. Mendes Filho, A. L. Zanin, M. H. Lente, and D. Garcia, J. Raman Spectrosc. **40**, 1144 (2009).
[32] E. K. H. Salje and U. Bismayer, Phase Transitions **63**, 1 (1997).
[33] J. Petzelt and V. Dvorak, J. Phys. C **9**, 1587 (1976).
[34] J. Petzelt and V. Dvorak, J. Phys. C **9**, 1571 (1976).
[35] U. Bismayer, Phase Transitions **27**, 211 (1990).
[36] J. Kreisel, G. Lucazeau, and H. Vincent, J. Solid State Chem. **137**, 127 (1998).
[37] J. Kreisel, H. Vincent, and G. Lucazeau, J. Raman Spectrosc. **30**, 115 (1999).
[38] P. Tarte, Spectrochim. Acta, Part A **23**, 2127 (1967).
[39] P. Tarte, A. Rulmont, M. Li'egeois-Duycckaerts, R. Cahay, and J. M. Winand, Solid State Ionics **42**, 177 (1990).
[40] E. Kroumova, M. I. Aroyo, J. M. Perez-Mato, A. Kirov, C. Capillas, S. Ivantchev, and H. Wondratschek, Phase Transitions **76**, 155 (2003).
[41] E. Husson, L. Abello, and A. Morell, Mater. Res. Bull. **25**, 539 (1990).
[42] U. Bismayer, V. Devarajan, and P. Groves, J. Phys. Condens. Matter **1**, 6977 (1989).
[43] A. Kania, K. Roleder, G. E. Kugel, and M. Hafid, Ferroelectrics **135**, 75 (1992).
[44] O. Svitelskiy, J. Toulouse, G. Yong, and Z.-G. Ye, Phys. Rev. B **68**, 104107 (2003).
[45] H. T. Stokes and D. M. Hatch, *Isotropy Subgroups of the 230 Crystallographic Space Groups* (World Scientific, Singapore, 1988).
[46] Y. Guo, H. Luo, D. Ling, H. Xu, T. He, and Z. Yin, J. Phys. Condens. Matter **15**, L77 (2003).
[47] Z. Li, Z. Xu, X. Yao, and Z.-Y. Cheng, J. Appl. Phys. **104**, 024112 (2008).
[48] D. Lin, Z. Li, S. Zhang, Z. Xu, and X. Yao, J. Appl. Phys. **108**, 034112 (2010).
[49] B. Noheda, D. E. Cox, G. Shirane, J. A. Gonzalo, L. E. Cross, and S.-E. Park, Appl. Phys. Lett. **74**, 2059 (1999).